European alternatives to design perforated thin-walled cold-formed beam–columns for steel storage systems

Claudio Bernuzzi *, Fabrizio Maxenti

Department of Architecture, Built Environment and Construction Engineering, Politecnico di Milano, Milano, Italy

Received 6 October 2014
Accepted 26 February 2015
Available online 4 April 2015

1. Introduction

Industrial steel storage pallet racks are quite similar to the framed steelworks traditionally used for civil and commercial buildings [1]: some differences are due to the presence of boltless beam-to-column connections with a moderate degree of flexural continuity and to the very extensive use of thin-walled cold-formed members, typically inter-ested by local and distortional buckling phenomena as well as by their mutual interaction [2]. Several types of storage systems are offered nowadays from manufacturers, such as adjustable pallet racks, which are the most commonly used (Fig. 1), drive-in and drive-through racks, push back racks, gravity flow racks and rack supported platforms. Serviceability responses and failure conditions are often complex to predict under both monotonic and seismic loads: in general, high engi-neering competences are required to guarantee significant load carrying capacities with structural systems of extremely limited weight, and, as a consequence, of very modest costs in order to be competitive on the market.

* Corresponding author. Tel.: +39 02 23994246.
E-mail address: claudio.bernuzzi@polimi.it (C. Bernuzzi).

Theory of thin-walled cold-formed members with open solid cross-section was well-established several decades ago [3–5] and now steel specifications propose very refined design approaches able to account for local, distortional and overall buckling phenomena as well as for their mutual interactions. Verification criteria adopted in Europe to design cold-formed beam–columns with a non-symmetric class 4 cross-section [6] impose the evaluation of five effective cross-sections: one for the axial load and four associated with flexure, being necessary to consider the cases of both positive and negative moments about each principal axis. The width of the effective compressed zones of the cross-section is significantly influenced [7,8] by the interaction between axial load and bending moments, which is ignored when evaluating the resisting cross-section properties. Moreover, with reference to storage racks, the uprights, i.e. the vertical beam–column members of the skel-eton frames, have generally an open mono-symmetric cross-section (Fig. 2), characterized by the presence of regular perforations to erect quickly the structures and/or to adapt the clear height of the load levels to the pallet sizes, which could change over time. Important theoretical and experimental studies have been focused on perforated plates and members. In particular, Szabo and Dubina [9] discussed accurately the existing cold-formed calculation methods to evaluate the strength and proposed an approach for members with square and circular holes. The same type of perforations was considered also in other studies on

Fig. 1. Typical adjustable pallet rack.

isolated plates [10–12], angles [13] and channels [14]. As to the uprights for adjustable pallet racks, recently Eccher et al. [15] proposed an isoparametric spline finite strip method for the geometric nonlinear analysis of perforated folded-plate structures. Moreover, important re-searches are currently in progress [16,17] to contribute to the develop-ment of appropriate design approaches able to account directly for the presence of perforations in columns and beam–columns. Furthermore, as clearly summarized in ref. [18], the existing rules to design racks are therefore empirical and their validity is only in the range of the in-vestigated parameters. In particular, from a practical point of view, due to the great differences not only in the cross-section upright geom-etries (Fig. 2) but also in their perforation types (Fig. 3), i.e. circular, el-liptic and diamond holes, slots and cut-outs, a design assisted by testing procedure is required by the most recent rack specifications [19–21]. The European code for cold-formed steel structures [22] proposes a very refined approach which cannot be used for uprights, owing to the complex cross-section shapes and to the presence of regular perfo-rations. Effective cross-section properties of uprights to be used for all the verification checks must hence be based on component tests, which are accurately described in the Appendix A of EN 15512 standard [19] for rack design in European areas. In particular, the stub column test allows to evaluate the effective area accounting for perforations, cold manufacturing processes, local and distortional buckling phenom-ena and their natural interactions. The typical specimen is composed by a stub upright, at each end of which a thick steel plate is welded (Fig. 4). The characteristic failure load (R_k) is based on the statistical re-elaboration of the experimental results related to a set of tests on nominally equal specimens under axial load: the effective area, A_{eff}, however limited to be not greater than the gross one, is evaluated as:

$$A_{eff} = \frac{R_k}{f_y} \tag{1}$$

where f_y is the yielding strength of the base material before the cold working processes.

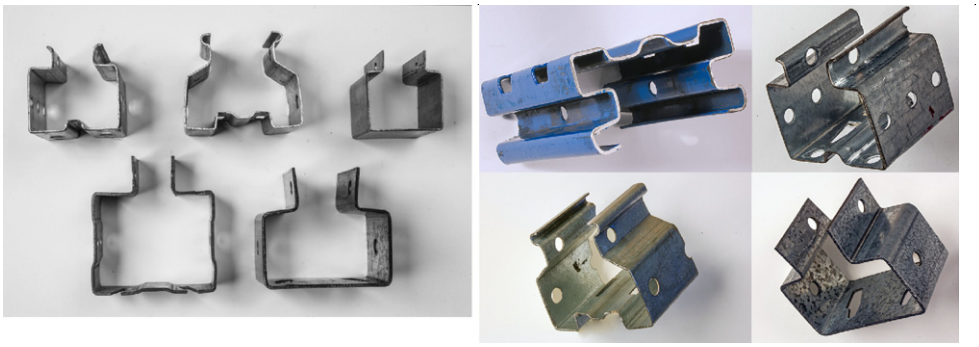

Fig. 2. Typical mono-symmetric cross-section employed as rack uprights (courtesy of Miss. Alessandra Pellegatto).

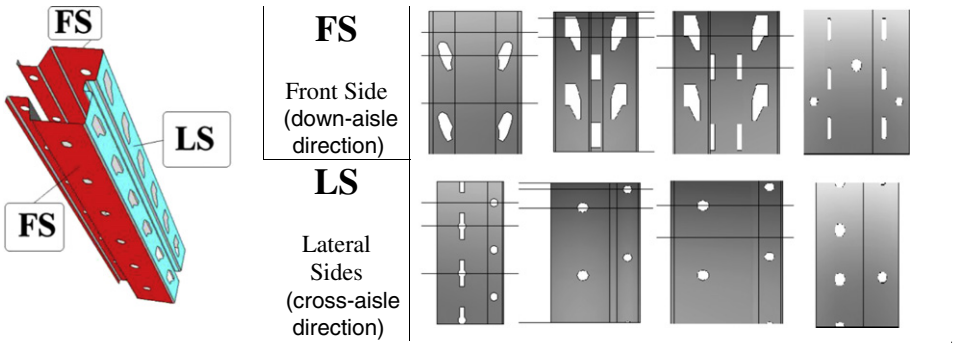

Fig. 3. Typical perforation systems for the rack uprights.

In a similar way, the bending tests allow for the prediction of the up-right flexural performances about major and minor axes of bending (Fig. 5): an adequate specimen length (L) is required to be not lower than 30 times the depth (D) of the upright to be tested. When the knowledge of the flexural member behavior is required about the axis of symmetry, a complete upright frame has to be tested instead of an isolated upright. The main result of these tests is the load–midspan displacement curve, from which the values of the effective second mo-ments of area and of the section moduli can be directly estimated.

A research project is currently in progress in Italy on the design ap-proaches for selective storage rack systems [23,24] and this paper sum-marizes a study aimed at comparing three European alternatives [6,19, 22] to evaluate the upright load carrying capacity. In addition to the standard provisions for steel storage pallet racks [19], also the part 1-3 [22] of Eurocode 3 has been considered and a quite innovative method (the so-called *general method*) proposed in the part 1-1 of EC3 [6] has been applied, which seems very promising because of the possibility to capture the key features of the perforated upright response avoiding component tests. Research outcomes related to solid members in class 3 have already been discussed [25]: the observed differences in terms of load carrying capacity reflect directly on the weight, and, as a conse-quence, on the cost of the overall racks. Now attention is paid on up-rights for adjustable pallet racks, i.e. on beam–column perforated members, for which more relevant differences between the three considered design alternatives are expected, owing to the different ways of taking into account for the presence of perforations.

2. The considered upright design cases

Selective steel storage pallet systems are spatial structures but major rack codes [19–21] admit for routine design their simplification in a set of independent plane frames lying in vertical planes, parallel and perpendicular to the aisles. Rack design is carried out following two separated steps:

- *structural analysis of the overall frame*, aimed at evaluating the set of displacements, internal forces and moments and stress distributions for each rack component;
- *member safety checks*, strictly depending on suitable criteria regarding deformability, resistance and stability.

This paper focuses on the second step and reference is made herein to the case of isolated beam–column with bending moments applied at member ends about the symmetry axis (y axis), considering hence the rack response in the down-aisle direction, which is, in general, the

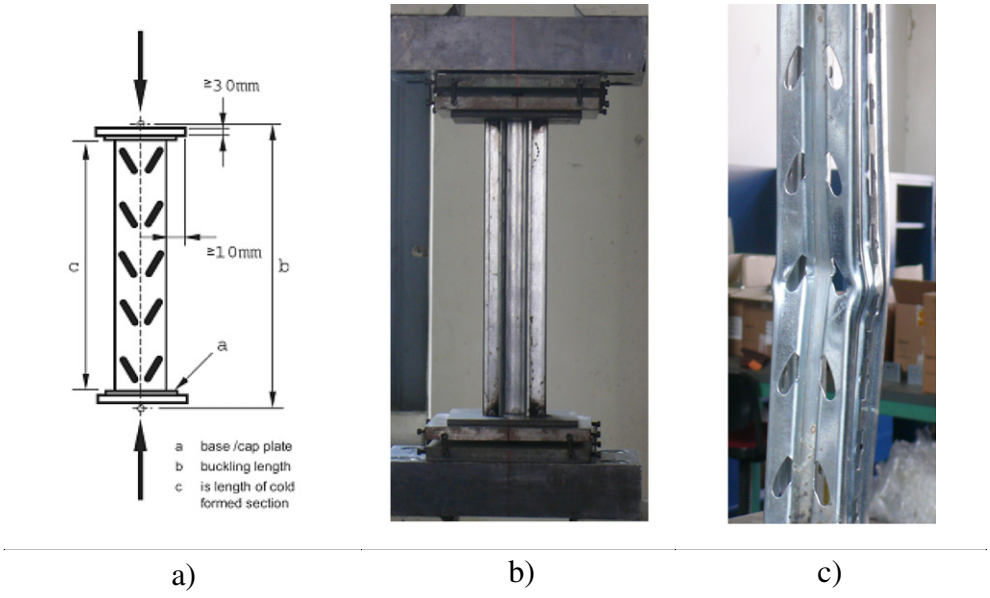

Fig. 4. Stub column test: details on the specimen (a), the specimen before testing (b) and the typical failure due to local and distortional buckling (c).

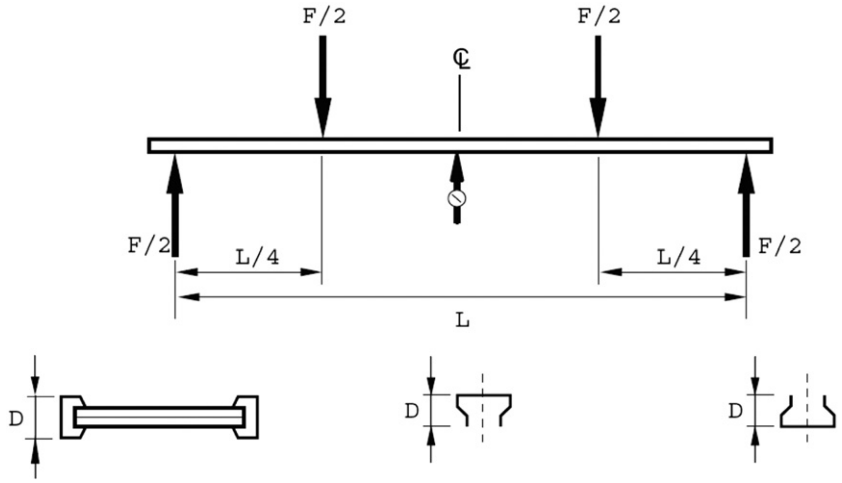

Fig. 5. Experimental arrangements for bending tests on upright section.

most critical for design purposes. The design analysis described in the paper has been carried out with reference to the following parameters:

- *the upright geometry*: three different cross-sections (Fig. 6) are considered, main data of which are presented in Table 1. With reference to the gross cross-section of each of them and to its material yielding strength (f_y), the squash load ($A \cdot f_y$) and the elastic bending moment ($W_y \cdot f_y$) are provided in order to allow a general appraisal of the member performances. Furthermore, the ratios between the second moments of area $\left(\frac{I_y}{I_z}\right)$, the section moduli ($\frac{W_y}{W_{z,\,inf}}$ and $\frac{W_y}{W_{z,\,sup}}$) and the radii of gyration $\left(\frac{\rho_y}{\rho_z}\right)$ are presented together with the uniform torsional and warping second moments of area (I_t and I_w, respectively) and the $\frac{y_0}{d}$ ratio, i.e. the eccentricity between the shear center and the centroid (y_0) over the distance between the centroid and the web (d). No additional data has been possible to add to the table because of the confidentiality required from manufactures for their patented products herein considered;
- *the load condition*: a constant axial load is combined with a gradient moment expressed by means of parameter ψ, i.e. the ratio between the minimum and the maximum end bending moment values (Fig. 7):

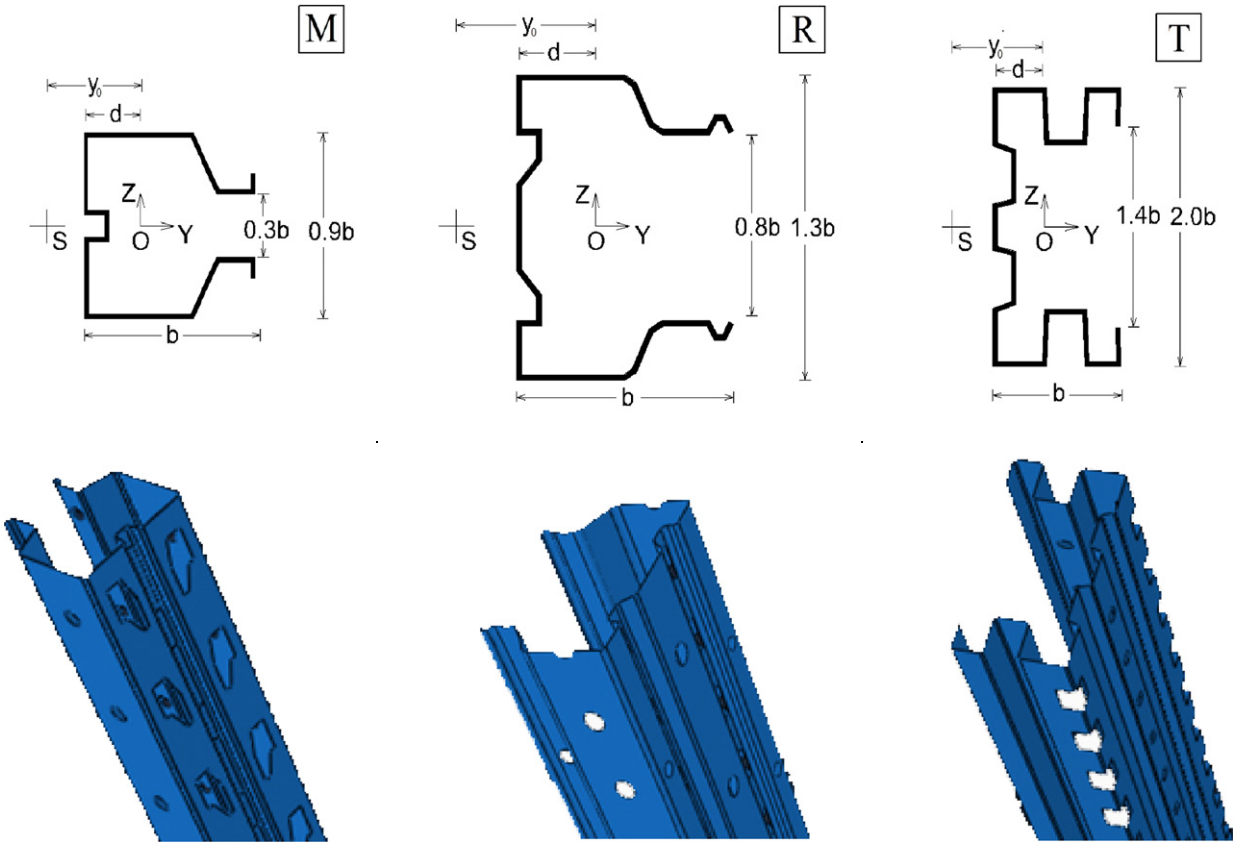

Fig. 6. The cross-sections considered in the present study.

Table 1
Key data of the considered cross section uprights.

Section properties	M	R	T
$A \cdot f_y$ [kN]	142.19	356.38	298.20
$W_y \cdot f_y$ [kNm]	3.22	13.32	10.74
I_y/I_z	0.995	2.200	5.350
$W_y/W_{z,\sup}$	1.18	2.18	2.99
$W_y/W_{z,\inf}$	0.93	1.20	2.27
y_0/d	2.306	2.253	1.989
I_t [mm^4]	619.01	2051.08	972.12
I_w [mm^6]	$1600 \cdot 10^6$	$5645 \cdot 10^6$	$630 \cdot 10^6$

$\psi = 1$ (uniform moment), $\psi = 0$ and $\psi = -1$ (opposite moments) values have been considered. Eccentricity (e) of the axial load with respect to the centroid in the cross-section subjected to the maximum moment has been considered by selecting values ranging from zero (column) to infinity (beam);

- *the member slenderness*: reference is made to three different values of the effective length (i.e. $L = 2$ m, 4 m and 5 m) of practical interest for routine rack design: the lowest is typical of rack braced in the down-aisle direction while the latter is associated with unbraced racks.

It should be noted that these selected upright cross-sections are characterized by geometrical properties significantly different, as it appears also from the values of the $\frac{I_y}{I_z}$ and $\frac{y_0}{d}$ ratios, ranging approximately from 1.0 to 5.3 and from 2 to 2.31, respectively. This choice allows an exhaustive overview of the cases most frequently encountered in routine rack design: the cross-section symmetry axis is the major axis for the T_upright and R_upright, as it generally occurs in rack practice; in case of M_uprights, $\frac{I_y}{I_z}$ and $\frac{\rho_y}{\rho_z}$ ratios are practically equal to unity (slightly lower) but these members behave remarkably different from the bi-symmetric ones, owing to the presence of a non-negligible shear center eccentricity $\left(\frac{y_0}{d} = 2,3\right)$.

Differences of the perforation systems can be appraised in Fig. 6: the hooks engage on the front-side into diamond and circular holes for M_ and R_uprights, respectively, while, for T_uprights, boxed slots are located across the corners between the front side and the lateral cross-section sides.

Major rack design codes [19–21] required to evaluate the effective cross-section properties by reducing the gross ones via suitable Q factors defined experimentally by the tests [19]. With reference to the verification checks for axial load and for bending moment, both $Q^N_{\exp} = \frac{A_{eff}}{A}$ and $Q^M_{\exp} = \frac{W_{eff,y}}{W_y}$ values, associated with stub column and bending tests, respectively, are reported in Table 2, which have been evaluated by the manufactures. In the same table, the $Q^N_{perf} = \frac{A_{perf}}{A}$ and $Q^M_{perf} = \frac{W_{perf,y}}{W_y}$ values are also presented, where subscript *perf* is related to the perforated cross-section of minimum area (net area). Differences between $Q^N_{\exp}$ and $Q^M_{\exp}$ are quite limited, approximately not greater than 3%. As to the reduction factor for the axial load, $Q^N_{\exp}$ is generally quite similar to Q^N_{perf} and the differences are lower than 4%; otherwise, the bending moment reduction factor $Q^M_{\exp}$ is significantly greater (up to 19%) than Q^M_{perf}.

3. Upright design in accordance with the European approaches

European design of steel storage pallet systems is usually carried out on the basis of the EN 15512 [19], which contains the basis for monotonic design. Furthermore, reference should be made also to the part 1-3 of EC3 [22], being uprights often cold-formed members. As already mentioned, a critical aspect is the evaluation of the effective cross-section properties: the well-established theoretical approach proposed for solid members by this code to account for local and distortional buckling by reducing cross-section geometric parameters cannot be directly applied to perforated uprights. As a consequence, the EN 15512 [19] testing procedure should be conveniently adopted to evaluate effective design parameters required by cold-formed specifications. Finally, as alternative, the *general method* of part 1-1 of EC3 [6] should be applied, which seems a very promising approach, owing to the possibility to take directly into account the presence of perforations via suitable numerical analyses. As already mentioned, attention is herein focused on the vertical elements of racks modeled as planar frames: uprights are considered loaded (Fig. 7) by an axial compression force, N_{Ed}, and a bending moment, $M_{y,Ed}$. It is worth to mention that, due to the use of thin-walled open cross-sections, uprights should also be prone to lateral torsional buck-ling, which has to be hence adequately considered in the design.

3.1. Verification in accordance with EN 15512

The following condition has to be fulfilled for the EN 15512 verifica-tion check of beam–columns:

$$\frac{N_{Ed}}{\chi_{\min} A_{eff} f_y/\gamma_M}\Bigg) + \frac{k_{LT} M_{y,Ed}}{\chi_{LT} W_{eff,y} f_y/\gamma_M}\Bigg) = (n) + \left(m_y\right) \leq 1 \tag{2}$$

in which χ is the reduction factor accounting for buckling phenomena, A and W_y are the area and the cross-section modulus about the principal cross-section symmetry (y) axis, respectively, f_y is the material yielding strength, subscript *eff* is related to the effective cross-section and γ_M is the material safety factor.

As to the axial load (term n in Eq. (2)), it is at first required to evaluate the relative slenderness $\overline{\lambda}$ defined as:

$$\overline{\lambda} = \sqrt{\frac{A_{eff} f_y}{N_{cr}}} \tag{3}$$

in which N_{cr} is the elastic critical load for the appropriate buckling mode (flexural, torsional or flexural–torsional), which can be determined via theoretical approaches [4,5] applied to the gross cross-section.

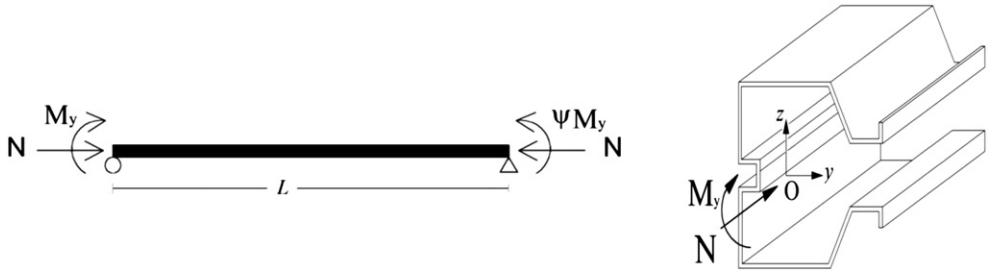

Fig. 7. The isolated member under gradient moment considered in the present analysis.

Table 2
Q-values for the considered cross-section uprights.

Section properties	M	R	T
$Q^N_{exp} = \frac{A_{eff}}{A}$	0.8014	0.8525	0.8130
$Q^N_{perf} = \frac{A_{perf}}{A}$	0.8025	0.8231	0.8225
$Q^M_{exp} = \frac{W_{eff}}{W}$	0.7905	0.8376	0.8412
$Q^M_{perf} = \frac{W_{perf}}{W}$	0.6669	0.7827	0.8096

In order to reduce the number of parameters affecting the research outcomes, it has been assumed that distortional buckling does not result critical. Buckling reduction factor χ is defined as:

$$\chi = \frac{1}{\left\{0.5\left[1+0.34(\overline{\lambda}-0.2)+\overline{\lambda}^2\right]\right\}+\sqrt{\left\{0.5\left[1+0.34(\overline{\lambda}-0.2)+\overline{\lambda}^2\right]\right\}^2-\overline{\lambda}^2}} \le 1. \tag{4}$$

As to the bending moment contribution (term m_y in Eq. (2)), the reduction factor for lateral–torsional buckling (χ_{LT}) is determined via Eq. (4) by substituting the relative slenderness for axial load ($\overline{\lambda}$) with the one for the beam lateral–torsional buckling ($\overline{\lambda}_{LT}$) defined as:

$$\overline{\lambda}_{LT} = \sqrt{\frac{W_{eff,y} f_y}{M_{cr}}} \tag{5}$$

where term M_{cr} is the elastic critical moment for lateral–torsional buckling, for which suitable equations are available in the literature [4,5].

Term k_{LT} is given by the expression:

$$k_{LT} = 1 - \frac{\mu_{LT} N_{Sd}}{\chi_z A_{eff} f_y} \le 1 \tag{6a}$$

with:

$$\mu_{LT} = 0.15 \cdot \left(\overline{\lambda}_z \beta_{M,LT} - 1\right) \le 0.9 \tag{6b}$$

where $\overline{\lambda}_z$ is the relative slenderness for flexural buckling about z axis (principal non-symmetry axis) and $\beta_{M,LT}$ is an equivalent uniform moment factor for lateral–torsional buckling, which can be approximated in case of bending moment with a linear variation as:

$$\beta_{M,LT} = 1.8 - 0.7\frac{M_{\min}}{M_{\max}} = 1.8 - 0.7 \cdot \psi \tag{7}$$

where M_{min} and M_{max} indicate the minimum and the maximum bending moments at the end of the element, respectively, with $\psi = \frac{M_{\min}}{M_{\max}}$.

It should be noted that this design approach has already been proposed in the previous version of EC3 (ENV version [26]) but it has been removed from the EN version [6] due to its inaccuracy [27], not only for members having mono-symmetric cross-section, but, in several cases, also for bi-symmetric beam–columns. Furthermore, no practical indications are given to designers for what concerns the elastic buckling interaction between axial force and bending moment. In routine design, this interaction is usually neglected: the proposed buckling reduction factors (χ) for beam–columns are evaluated with reference to the cases of axial load ($\chi_{\min}$) and bending moment (χ_{LT}). From a practical point of view, an extremely non-conservative elastic critical domain is assumed (Fig. 8): the reduction of the buckling moment due to the presence of the axial load is ignored, despite the fact that recent studies [28,29] have stressed out its non-negligible influence.

3.2. Verification in accordance with EN 1993-1-3

As alternative, reference can be made to the European approach recommended for the design of cold-formed thin-walled beam–columns subjected to mono-axial bending. In part 1-3 of EC3 [22] the following equation is proposed:

$$\left(\frac{N_{Ed}}{N_{b,Rd}}\right)^{0.8} + \left(\frac{M_{Ed}}{M_{b,Rd}}\right)^{0.8} = (n)^{0.8} + \left(\frac{m_y}{k_{LT}}\right)^{0.8} \le 1 \tag{8}$$

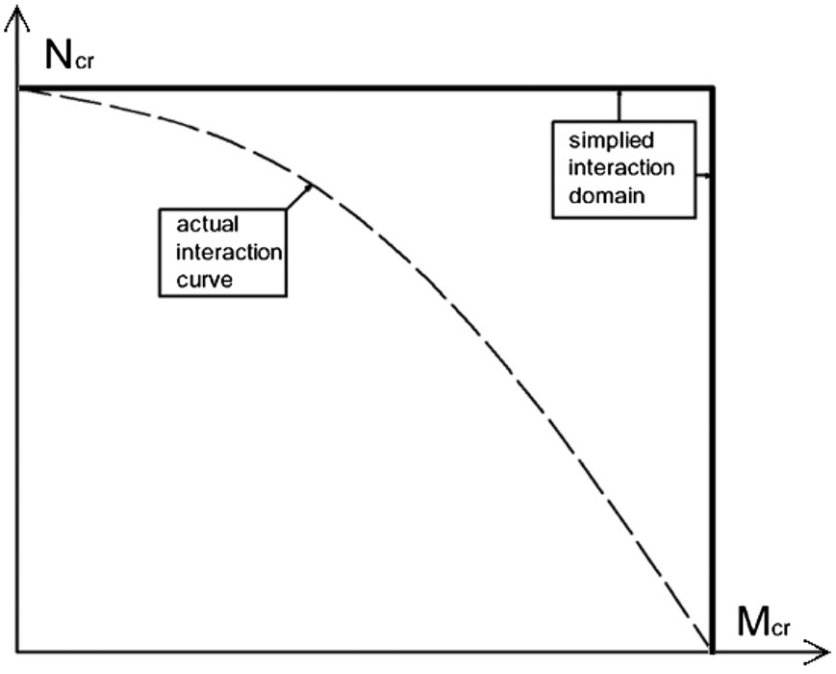

Fig. 8. Typical interaction buckling domain for beam–column: the actual domain and the non-conservative proposed design domain.

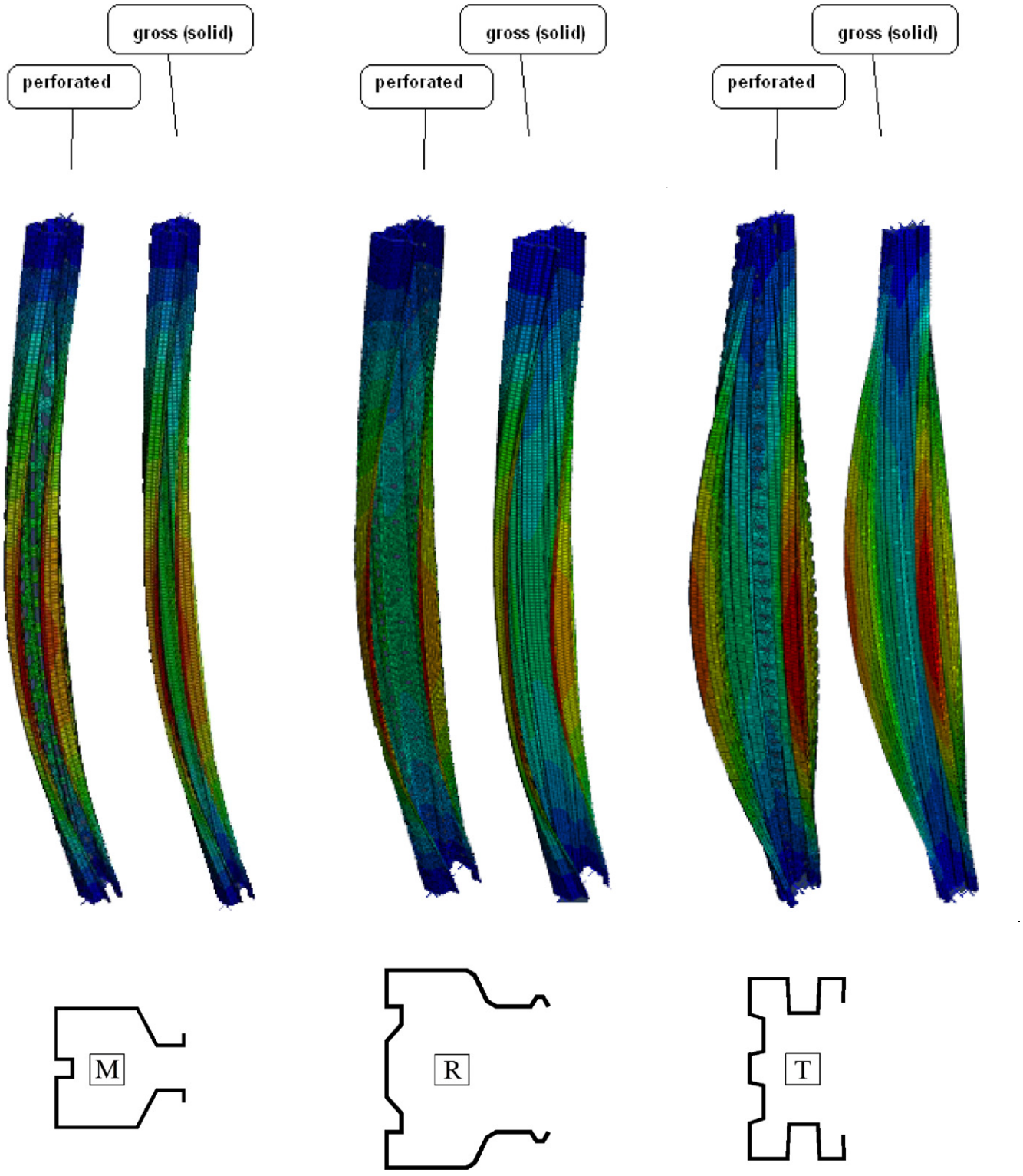

Fig. 9. Typical buckling shapes under axial load for the considered solid and perforated uprights ($L = 2$ m).

where $N_{b,Rd}$ is the column design buckling resistance and $M_{b,Rd}$ is the beam design bending moment resistance, accounting for lateral buckling.

Owing to the absence of rules to evaluate the effective cross-section properties of perforated members, both $N_{b,Rd}$ and $M_{b,Rd}$ are evaluated via the same equations recommended in EN 15512: the only difference

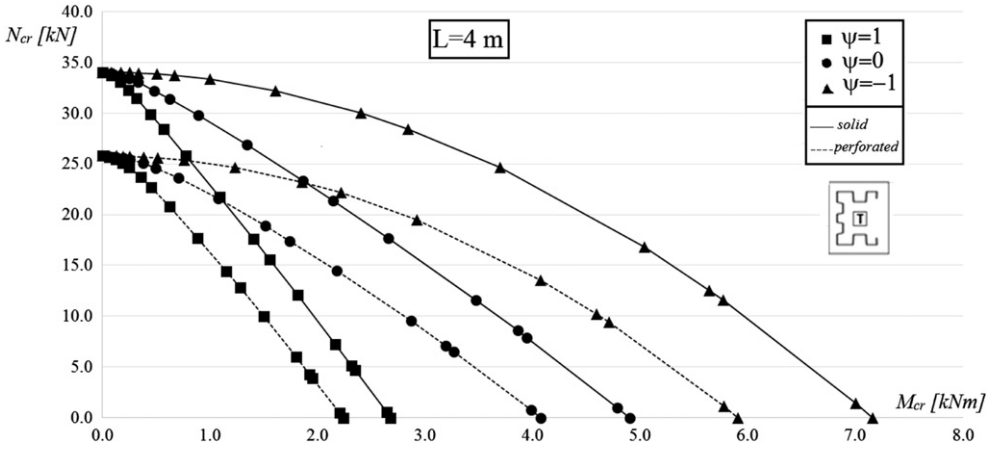

Fig. 10. Typical N_{cr}–M_{cr} buckling interaction domains for the solid (solid line) and the perforated (dashed line) uprights: the cases of T_uprights with $L = 4$ m.

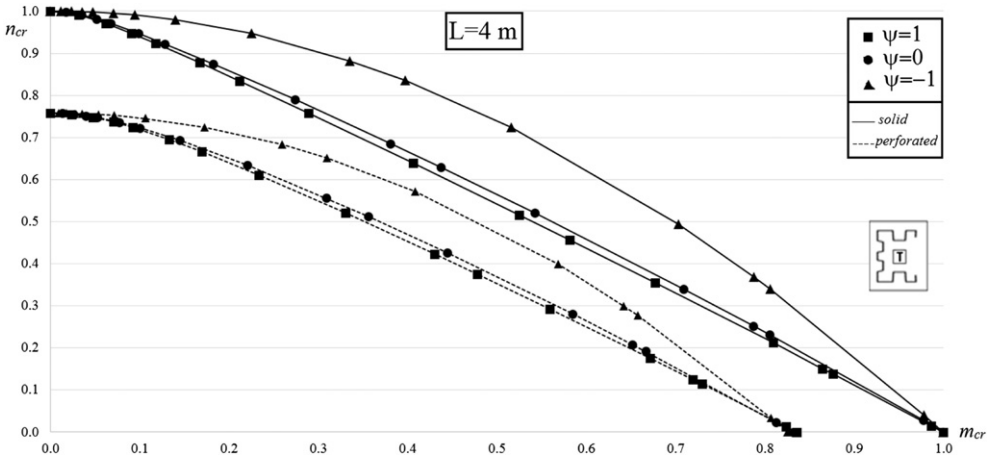

Fig. 11. Typical non-dimensional n_{cr}–m_{cr} buckling interaction domains for the solid (solid line) and the perforated (dashed line) uprights: the cases of T_uprights with $L = 4$ m.

from Eq. (2) is the presence of the exponent 0.8 and the absence of term k_{LT} in the m_y contribution.

3.3. Verification in accordance with EN 1993-1-1

Eurocode 3 in its part 1-1 [6] proposes an innovative [30–32] design approach, the so-called *general method*, for the stability checks of structural components having geometrical, loading and/or supporting irregularities. Overall buckling resistance is verified when:

$$\frac{\chi_{op}\alpha_{ult,k}}{\gamma_M} \geq 1 \tag{9}$$

where $\alpha_{ult,k}$ is the minimum load multiplier evaluated with reference to the cross-section resistance, χ_{op} is the buckling reduction factor referred to the overall structural system and γ_M is the material safety factor.

For routine design, upright cross-sections in classes 3 or 4 guarantee that plastic hinges don't form in the members. Overall failure is general-ly due to the interactions between upright instability and plasticity in the beam-to-column joints and in the base–plate connections, as also confirmed by a recent experimental research which included several full scale push-over rack tests [33]. Ultimate load multiplier for resistance, $\alpha_{ult,k}$ is determined as:

$$\frac{1}{\alpha_{ult,K}} = \frac{N_{Ed}}{N_{Rk}} + \frac{M_{y,Ed}}{M_{y,Rk}}. \tag{10}$$

where N_{Rk} and $M_{y,Rk}$ are the squash load and the first yielding moment, respectively, of the perforated cross-section.

Buckling reduction factor χ_{op} can be evaluated via Eq. (4) on the basis of relative slenderness $\overline{\lambda}_{op}$ of the whole structure defined as:

$$\overline{\lambda}_{op} = \sqrt{\frac{\alpha_{ult.k}}{\alpha_{cr,op}}} \tag{11}$$

where $\alpha_{cr,op}$ is the minimum buckling multiplier.

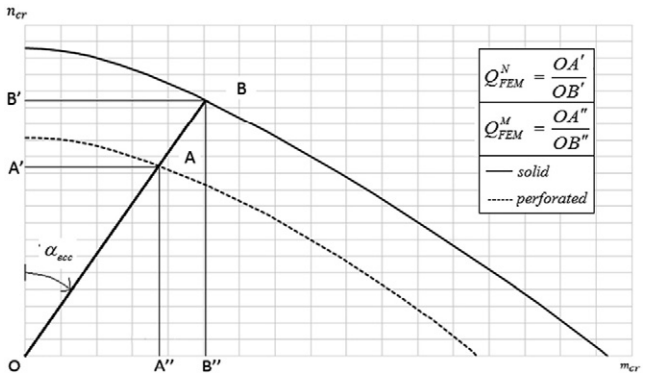

Fig. 12. Definition of the numerical reduction factors for the area (Q^N_{FEM}) and for the section modulus (Q^M_{FEM}).

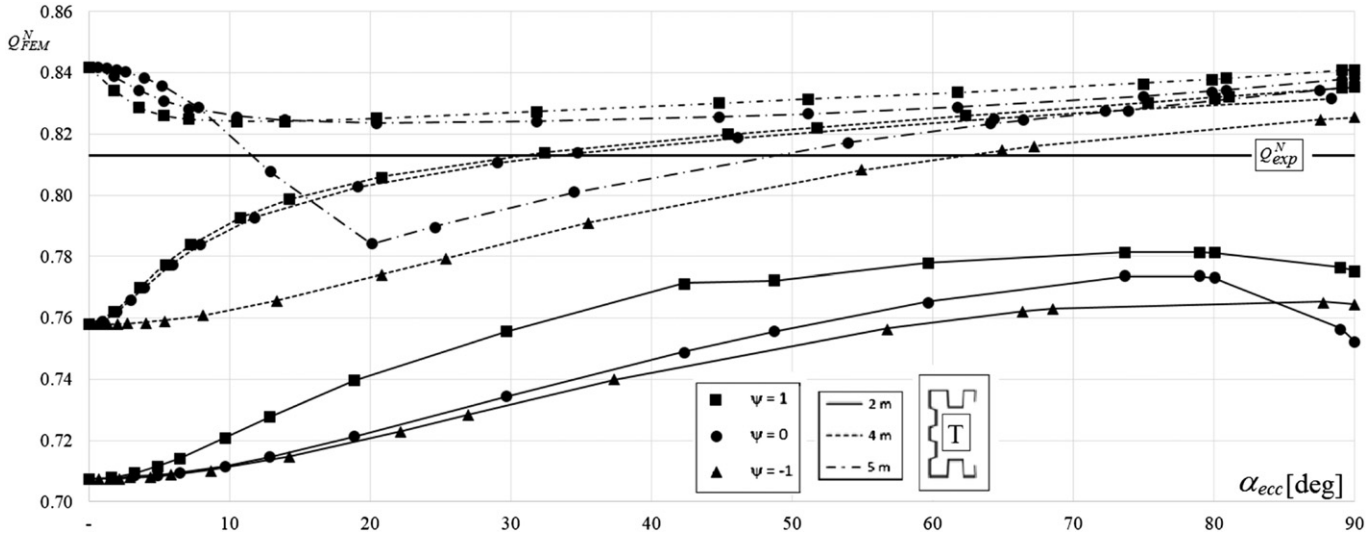

Fig. 13. $Q^N_{FEM} - \alpha_{ecc}$ relationships for all the cases related to the T_uprights.

It is worth to mention that this approach seems very promising when applied to racks. A non-negligible advantage of the *general meth-od* with respect to the other two alternatives consists in the fact that only FE numerical analyses and/or analytical computations are required, avoiding hence stub column and beam tests. Despite very refined FE beam formulations that are nowadays available to model cold-formed thin walled members [34–45], the buckling analysis of the perforated beam–columns can be carried out via commercial (and economical) finite element analysis programs to model the uprights by means of elastic shell elements: in this way the influence of the perforation sys-tems reflects directly on the critical load multiplier $\alpha_{cr,op}$. Moreover, also the term $\alpha_{ult,k}$, which is related to the attainment of the yielding of the most stressed point of the net cross-section under axial load and bending moment, can be estimated directly.

4. Influence of the perforation systems on the elastic buckling

The two design approaches for cold-formed beam–column members (i.e. EN 15512 and EC3 1-3) require the evaluation of both the buckling load for compression and the critical bending moment for flexure, which can be determined numerically or theoretically on the basis of the gross cross-section geometries. On the contrary, the general method proposed by EC3 1-1 requires the value of the buckling load of the per-forated members, which cannot be appreciated theoretically, owing to the absence of suitable formulations accounting for the presence of perforations. As a consequence, in the following reference is made to nu-merical buckling analysis results obtained by using the commercial analysis software ABAQUS [46], meshing accurately the uprights with S4R elastic shell elements to consider adequately the presence of the

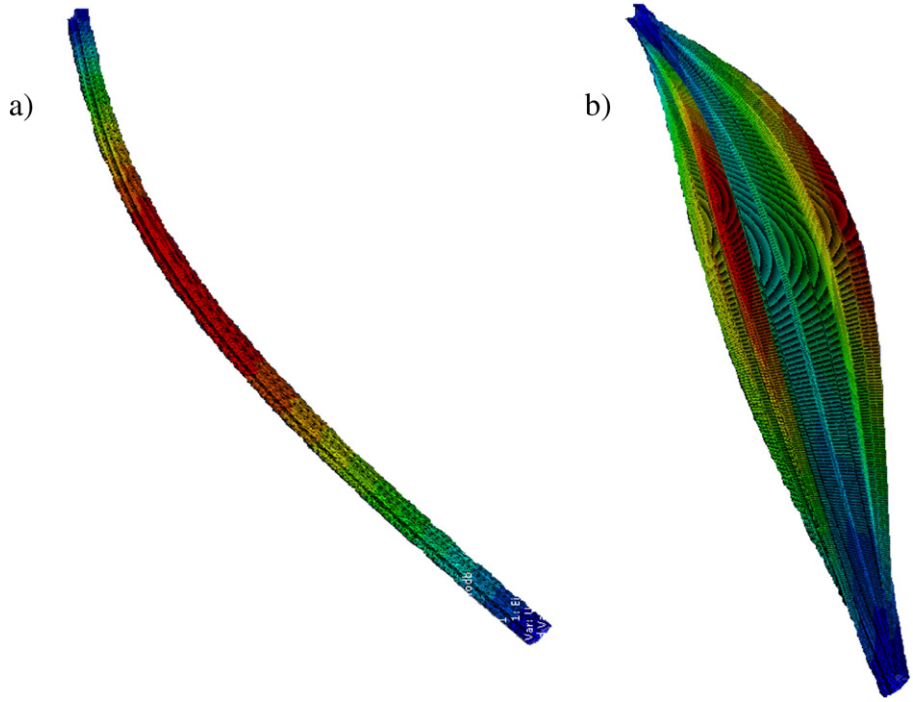

Fig. 14. Typical deformed shapes for flexural (a) and flexural–torsional buckling (b) in case of T_uprights with $L = 5$ m and $\psi = 0$.

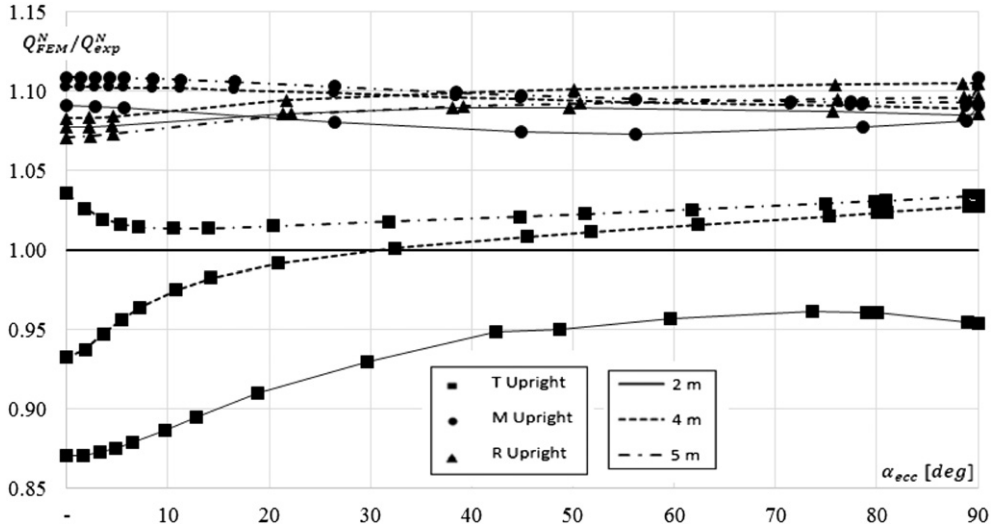

Fig. 15. $Q^N_{FEM}/Q^N_{exp} - \alpha_{ecc}$ relationships for all the considered cases with $\psi = 1$.

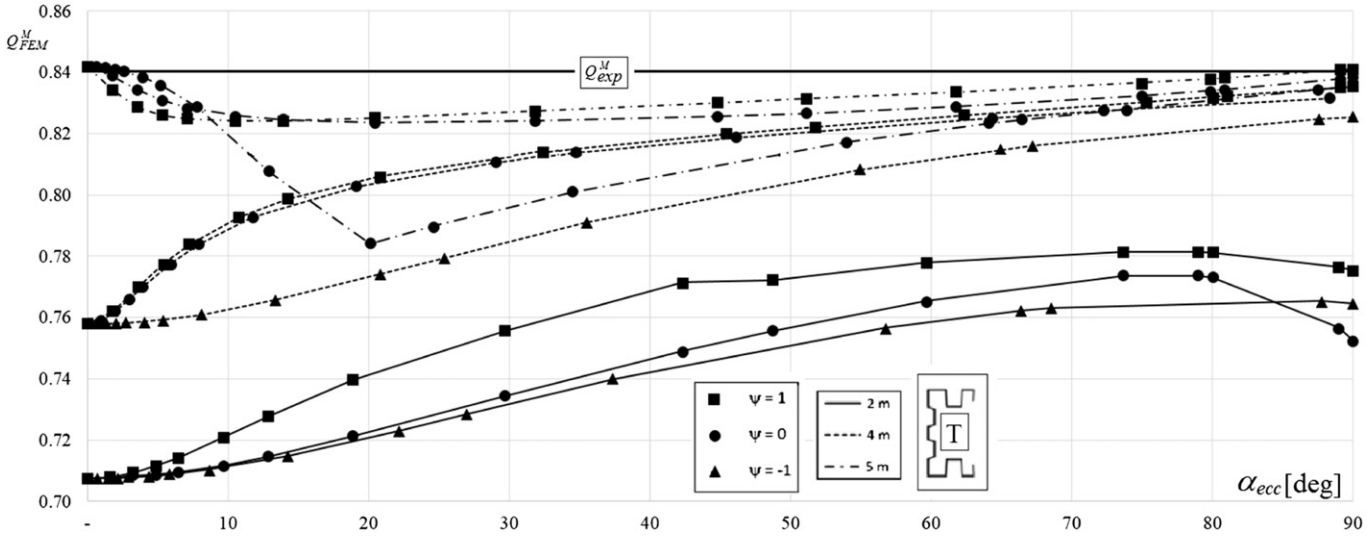

Fig. 16. $Q^M_{FEM} - \alpha_{ecc}$ relationships for all the cases related to the T_uprights.

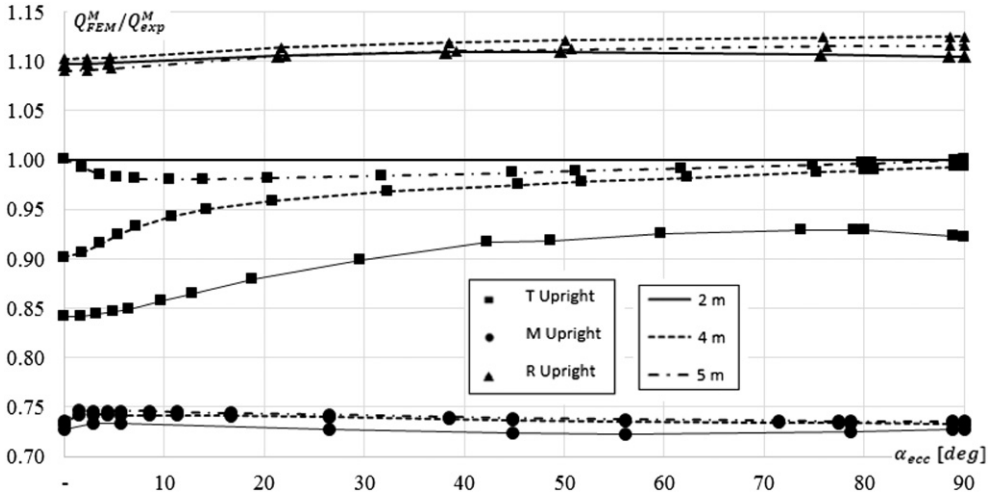

Fig. 17. $Q^M_{FEM}/Q^M_{exp} - \alpha_{ecc}$ relationships for all the considered cases with $\psi = 1$.

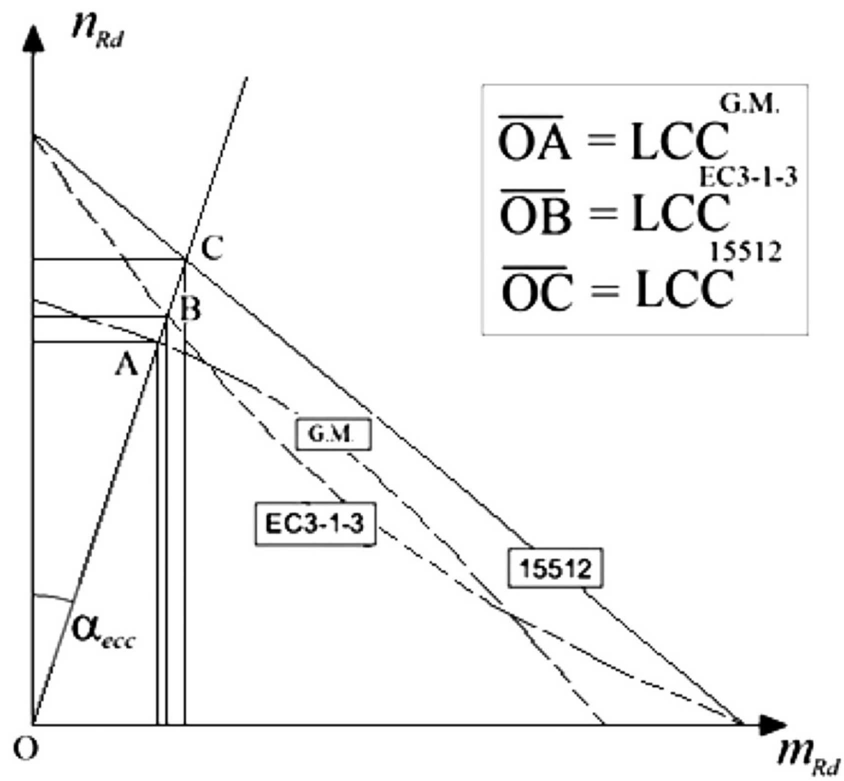

Fig. 18. Definition of the load carrying capacity (LCC^L) and definition of the eccentricity angle α_{ecc}.

perforations (Fig. 6). In order to reproduce the supported boundary con-ditions a mask at each member end was applied via three independent wire elements, restrained to each other in order to allow free warping of the end cross-sections. Furthermore, the same uprights have been modeled also as solid members, despite the fact that the available theo-retical approaches [28,29] predict accurately their buckling loads [25]. As an example, the buckling shape for the solid and perforated columns for each upright with $L = 2$ m are presented in Fig. 9. Buckling is due to the interaction between flexure and torsion and the presence of perfora-tions, as expected, reduces significantly the cross-section in-plane stiff-ness, increasing the relative rotation between the flanges and the web. The discussed outcomes based on a number of load cases enough to reproduce the critical N_{cr}–M_{cr} domains with satisfactory accuracy have been considered: Fig. 10 refers to T_upright with $L = 4$ m under three different bending moment distributions: solid and dashed lines are re-lated to the solid and perforated cross-section domains, respectively. It can be noted that the typical critical domain is convex, similar to the one proposed in Fig. 8 to underline, once again, the non-negligible over-estimation associated with the traditional design assumptions. It seems convenient to consider the non-dimensional buckling domains to allow a direct appraisal of the influence of the perforations on the buckling loads: Fig. 11 presents the data already plotted in Fig. 10 here proposed in the non-dimensional n_{cr}–m_{cr} reference system, being n_{cr} and m_{cr} defined with respect to the gross (solid) cross-section (subscript *gr*) as:

$$n_{cr}(M) = \frac{N_{cr}(M)}{N_{cr,gr}(M=0)} \tag{12a}$$

$$m_{cr}(M) = \frac{M_{cr}(N)}{M_{cr,gr}(N=0)}. \tag{12b}$$

When N_{cr} and M_{cr} are related to perforated members, these non-dimensional domains allow to define directly a new geometrical reduc-tion factor, identified in the following as $Q_{\ FEM}$. This term accounts for the sole geometrical discontinuities, being neglected the post-elastic be-havior and hardening resources of the material due to cold-formed working processes. From this elastic numerical reduction factor, two dif-ferent contributions can be conveniently identified (Fig. 12): Q^N_{FEM} and Q^M_{FEM}, associated with the axial load and the bending moment, respec-tively: the generic load case of interest can be uniquely identified via a

Table 3
M_uprights: value of the $\frac{LCC^{15512}}{LCC^{EC3\text{-}1\text{-}3}}$, $\frac{LCC^{G.M.}}{LCC^{15512}}$ and $\frac{LCC^{G.M.}}{LCC^{EC3\text{-}1\text{-}3}}$ ratios.

e [mm]	$L = 2$ m			$L = 4$ m			$L = 5$ m		
	$\frac{LCC^{15512}}{LCC^{EC3\text{-}1\text{-}3}}$	$\frac{LCC^{G.M.}}{LCC^{15512}}$	$\frac{LCC^{G.M.}}{LCC^{EC3\text{-}1\text{-}3}}$	$\frac{LCC^{15512}}{LCC^{EC3\text{-}1\text{-}3}}$	$\frac{LCC^{G.M.}}{LCC^{15512}}$	$\frac{LCC^{G.M.}}{LCC^{EC3\text{-}1\text{-}3}}$	$\frac{LCC^{15512}}{LCC^{EC3\text{-}1\text{-}3}}$	$\frac{LCC^{G.M.}}{LCC^{15512}}$	$\frac{LCC^{G.M.}}{LCC^{EC3\text{-}1\text{-}3}}$
0	1.000	0.905	0.904	1.000	0.892	0.892	1.000	0.895	0.895
5	1.103	0.943	1.040	1.057	0.913	0.965	1.049	0.912	0.956
10	1.134	0.970	1.100	1.085	0.932	1.011	1.075	0.927	0.996
50	1.189	0.991	1.178	1.170	0.996	1.165	1.159	0.976	1.131
100	1.173	0.948	1.112	1.189	0.975	1.159	1.185	0.950	1.126
150	1.154	0.921	1.062	1.187	0.939	1.115	1.189	0.911	1.083
500	1.089	0.864	0.941	1.139	0.825	0.939	1.151	0.785	0.903
5000	1.020	0.834	0.851	1.038	0.750	0.778	1.044	0.697	0.728
∞	1.000	0.841	0.841	1.000	0.764	0.764	1.000	0.716	0.716

Table 4

R_uprights: value of the $\frac{LCC^{15512}}{LCC^{EC3\text{-}1\text{-}3}}$, $\frac{LCC^{G.M.}}{LCC^{15512}}$ and $\frac{LCC^{G.M.}}{LCC^{EC3\text{-}1\text{-}3}}$ ratios.

e [mm]	$L=2$ m			$L=4$ m			$L=5$ m		
	$\frac{LCC^{15512}}{LCC^{EC3\text{-}1\text{-}3}}$	$\frac{LCC^{G.M.}}{LCC^{15512}}$	$\frac{LCC^{G.M.}}{LCC^{EC3\text{-}1\text{-}3}}$	$\frac{LCC^{15512}}{LCC^{EC3\text{-}1\text{-}3}}$	$\frac{LCC^{G.M.}}{LCC^{15512}}$	$\frac{LCC^{G.M.}}{LCC^{EC3\text{-}1\text{-}3}}$	$\frac{LCC^{15512}}{LCC^{EC3\text{-}1\text{-}3}}$	$\frac{LCC^{G.M.}}{LCC^{15512}}$	$\frac{LCC^{G.M.}}{LCC^{EC3\text{-}1\text{-}3}}$
0	1.001	0.940	0.940	1.000	0.929	0.929	1.000	0.918	0.918
5	1.090	0.964	1.051	1.066	0.960	1.023	1.062	0.949	1.008
10	1.127	0.980	1.104	1.098	0.985	1.082	1.093	0.973	1.063
50	1.189	1.002	1.192	1.179	1.050	1.238	1.176	1.032	1.214
100	1.178	0.989	1.165	1.189	1.043	1.240	1.189	1.027	1.222
150	1.161	0.978	1.136	1.182	1.029	1.215	1.184	1.016	1.203
500	1.096	0.951	1.043	1.124	0.979	1.101	1.130	0.973	1.099
5000	1.022	0.935	0.956	1.032	0.943	0.974	1.034	0.939	0.971
∞	1.000	0.933	0.933	1.000	0.938	0.938	1.000	0.935	0.935

suitable eccentricity angle, α_{ecc}, ranging from zero (column) to infinite (beam). In Fig. 13, the $Q^N_{FEM} - \alpha_{ecc}$ relationships are plotted for the T_uprights together with the experimental stub column test value, which is unique and corresponds to a horizontal line, independent on the member length and the axial load eccentricity. The range of variation of Q^N_{FEM} is between 0.71 and 0.84 approximately and the lowest values are associated with the $L = 2$ m cases; the values for $\psi = 1$ are generally greater than the ones associated with $\psi = -1$. Increasing α_{ecc}, the value of the numerical reduction factor monotonically increases too, except for the longest members ($L = 5$ m): in these cases, the $Q^N_{FEM} - \alpha_{ecc}$ relationships present the minimum constant values extended for a wide range of axial load eccentricities. Furthermore, it is possible to observe a remarkably different trend with respect to the other plotted curves when $\psi = 0$, mainly due to the change of the critical buckling mode: flexural (Fig. 14a) for the lowest value of α_{ecc}, otherwise flexural–torsional (Fig. 14b).

To better appraise the substantial difference between the numerical values of the reduction factor and the ones obtained from stub column tests ($Q^N_{\exp}$), Fig. 15 proposes the same data as $Q^N_{FEM}/Q^N_{\exp} - \alpha_{ecc}$ relationships: the buckling values (Q^N_{FEM}) are greater (up to 11%) than the experimental ones except than for the T_upright with a $L = 2$ m and $L = 4$ m, reaching $Q^N_{FEM}/Q^N_{\exp}$ the value of 0.87 and 0.93, respectively.

With the same T_upright cases already considered in Fig. 13, attention has been paid to the bending contribution and Fig. 16 plots the $Q^M_{FEM} - \alpha_{ecc}$ relationships, which have a trend very similar to the $Q^N_{FEM} - \alpha_{ecc}$ ones. The experimental reduction factor for the bending moments (horizontal line) is always greater than the numerical one and these differences decrease in general with the increase of both α_{ecc} and L. Fig. 17 proposes the same cases of Fig. 15 plotting the $Q^M_{FEM}/Q^M_{\exp} - \alpha_{ecc}$ relationships: it can be noted that the experimental bending test approach provides always more favorable values of the reduction factor, except for R_uprights, independently on the member length: overestimation due to the numerical analysis is approximately constant and never greater than 13%.

5. Application of the design approaches

To allow a direct comparison between the three discussed design alternatives, the associated resisting domains can be considered, which are obtained via Eqs. (2), (8) or (9) by imposing the unity as results of the verification checks. Reference can be conveniently made to the value of the non-dimensional load carrying capacity (LCC^L), defined (Fig. 18) for the generic design method (superscript L), as:

$$LCC^L = \sqrt{\left(n^L_{Rd}\right)^2 + \left(m^L_{Rd}\right)^2}. \tag{13}$$

All the results related to the case of uniform moment ($\psi = 1$) are presented in Tables 3 (M_uprights), 4 (R_uprights) and 5 (T_uprights), in terms of $\frac{LCC^{15512}}{LCC^{EC3\text{-}1\text{-}3}}$, $\frac{LCC^{G.M.}}{LCC^{15512}}$ and $\frac{LCC^{G.M.}}{LCC^{EC3\text{-}1\text{-}3}}$ ratios. These data can be considered adequately representative also for all the other load cases (i.e. $\psi = 0$ and $\psi = -1$) not directly reported in the following, owing to the need of limiting the length of the paper.

As expected, $\frac{LCC^{15512}}{LCC^{EC3\text{-}1\text{-}3}}$ ratios are equal to unity when $e = 0$ and $e = \infty$, being the considered verification criteria different only for the beam–column cases. The EN 15512 approach leads in general to the greatest values (up to 19%, approximately) of the load carrying capacity: the differences between LCC^{15512} and $LCC^{EC3\text{-}1\text{-}3}$ are mainly in correspondence of eccentricity values ranging between 50 mm and 150 mm and appear modestly influenced by the beam–column member length.

In a previous research on class 3 uprights [25], it has been demonstrated that the *general method* appears as the most favorable one, giving a concave domain with load carrying capacity values associated with column and beam cases coincident with the ones obtained from the EN 15512 (linear beam–column domain) and the EC3-1-3 (convex domain). Otherwise, when perforated profiles are considered, the *general method* appears as the most severe for the limit cases of column and beam: differences with respect to the performances guaranteed by the design rules for cold-formed ($LCC^{EC3\text{-}1\text{-}3}$) and rack structures ($LCC^{15512}$) are non-negligible: approximately up to 25% for T_uprights in case of pure axial load and up to 28% for M_uprights under bending

Table 5

T_uprights: value of the $\frac{LCC^{15512}}{LCC^{EC3\text{-}1\text{-}3}}$, $\frac{LCC^{G.M.}}{LCC^{15512}}$ and $\frac{LCC^{G.M.}}{LCC^{EC3\text{-}1\text{-}3}}$ ratios.

e [mm]	$L=2$ m			$L=4$ m			$L=5$ m		
	$\frac{LCC^{15512}}{LCC^{EC3\text{-}1\text{-}3}}$	$\frac{LCC^{G.M.}}{LCC^{15512}}$	$\frac{LCC^{G.M.}}{LCC^{EC3\text{-}1\text{-}3}}$	$\frac{LCC^{15512}}{LCC^{EC3\text{-}1\text{-}3}}$	$\frac{LCC^{G.M.}}{LCC^{15512}}$	$\frac{LCC^{G.M.}}{LCC^{EC3\text{-}1\text{-}3}}$	$\frac{LCC^{15512}}{LCC^{EC3\text{-}1\text{-}3}}$	$\frac{LCC^{G.M.}}{LCC^{15512}}$	$\frac{LCC^{G.M.}}{LCC^{EC3\text{-}1\text{-}3}}$
0	1.000	0.744	0.744	1.000	0.772	0.772	1.000	0.850	0.850
5	1.077	0.781	0.842	1.075	0.808	0.868	1.073	0.863	0.926
10	1.112	0.812	0.903	1.109	0.828	0.918	1.107	0.866	0.958
50	1.187	0.899	1.066	1.185	0.861	1.021	1.184	0.872	1.032
100	1.186	0.905	1.073	1.186	0.865	1.026	1.187	0.870	1.033
150	1.174	0.899	1.055	1.175	0.864	1.015	1.176	0.868	1.021
500	1.110	0.871	0.966	1.113	0.857	0.954	1.115	0.859	0.958
5000	1.028	0.845	0.869	1.028	0.851	0.874	1.029	0.853	0.877
∞	1.000	0.842	0.842	1.000	0.850	0.850	1.000	0.851	0.851

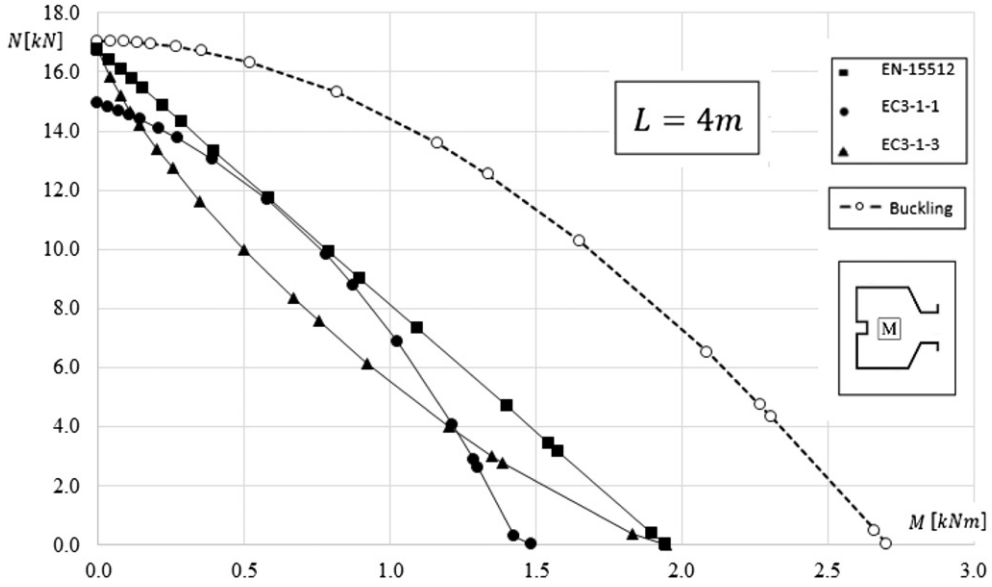

Fig. 19. M_uprights: resistance domains deriving from the application of the considered design methods ($\psi = 1$).

moment. These differences decrease for the beam–column cases: the trend of both the $\frac{LCC^{G.M.}}{LCC^{15512}}$ and $\frac{LCC^{G.M.}}{LCC^{EC3\text{-}1\text{-}3}}$ ratios is quite similar and the value of these ratios increases from the limit cases (e = 0 and e = ∞), reaching a maximum when eccentricity is comprised between 50 mm and 100 mm. A more severe prediction of the load carrying capacity can be noted when the general method is compared with the EN 15512 approach: the maximum values of $\frac{LCC^{G.M.}}{LCC^{15512}}$ ratio tend to unity, exceeding slightly (up to 5%) this value only for few R_upright cases. Furthermore, if the EN 1993-1-3 is considered, the $\frac{LCC^{G.M.}}{LCC^{EC3\text{-}1\text{-}3}}$ ratio presents a general trend similar to the $\frac{LCC^{G.M.}}{LCC^{15512}}$ one but the values are significantly greater: ratio $\frac{LCC^{G.M.}}{LCC^{EC3\text{-}1\text{-}3}}$ exceeds in many cases the unity, up to 19% approximately for M_ and T_uprights.

To better appraise the differences associated with these design approaches, the beam–column domains have been directly overlapped. As examples representative of all the considered cases, Figs. 19–21 can be considered for $L = 4$ m under constant moment; moreover, in the same figures also the critical domain obtained via FE elastic buckling analyses on the perforated uprights is plotted, too. For all the uprights it is obviously expected that the elastic critical domains are always larg-er than the design ones, independently on the considered approach, member length and load cases, due to the assumption of no limitation on material strength, as it appears clearly only from Figs. 19 to 20, which are related respectively to the M_ and R_uprights. Furthermore, if the T_uprights are considered (Fig. 21a), it results that both EN 15512 and EC3 1-3 approaches lead to evaluate a load carrying capacity surprisingly greater than the elastic critical buckling load for the column and beam–columns with the lowest values of the eccentricity, as it can be more clearly appreciated via the zoom in Fig. 21b. On the contrary, the domain associated with the general method is always within the elastic critical one for each considered case.

Owing to this unexpected overestimation of the resistance, more attention has been devoted to all the cases related to the T_uprights

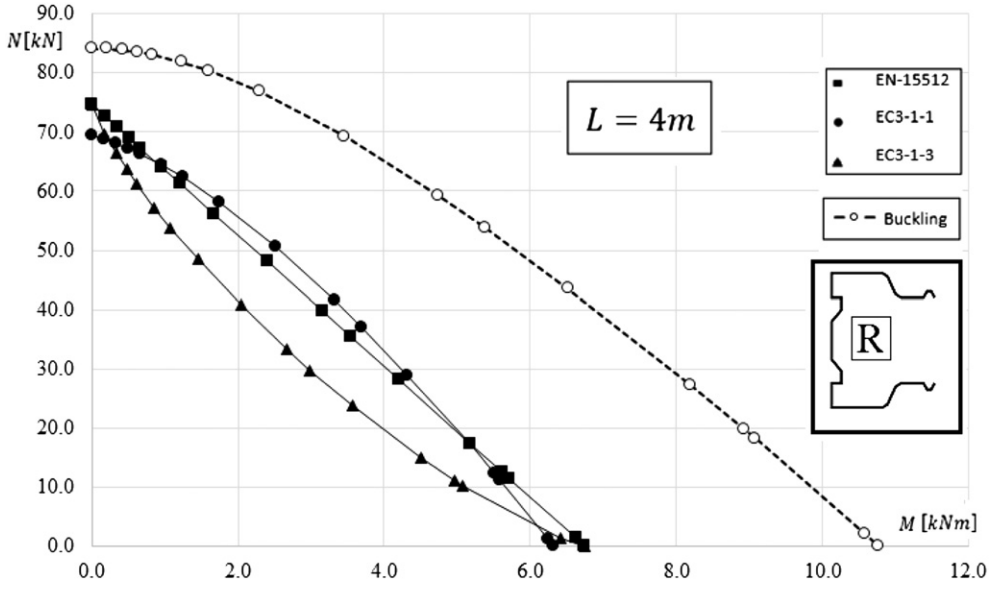

Fig. 20. R_uprights: resistance domains deriving from the application of the considered design methods ($\psi = 1$).

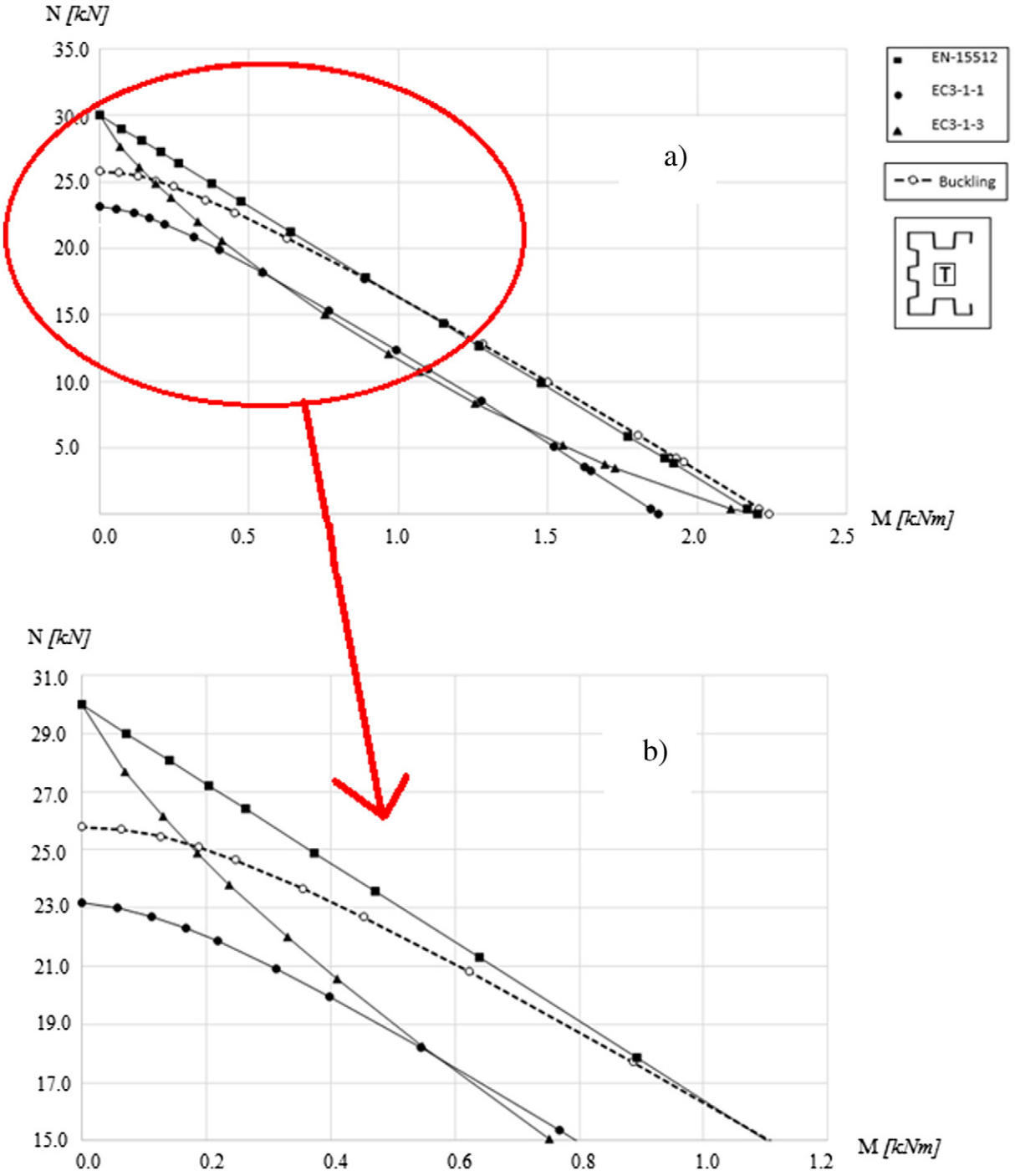

Fig. 21. T_uprights: resistance domains (a) deriving from the application of the considered design methods in case of $L = 4$ m ($\psi = 1$) and zoom (b) of the zone of interest.

and reference can be made to Table 6, where the $\frac{LCC^{15512}}{LCC^{FEM}}$, $\frac{LCC^{EC3\text{-}1\text{-}3}}{LCC^{FEM}}$ and $\frac{LCC^{G.M.}}{LCC^{FEM}}$ ratios are presented, being LCC^{FEM} load carrying capacity associated with the elastic buckling analysis. These data confirm the unsafe prediction of EN 15512 and EC3 1-3 approaches for low eccentricity values, independently on the moment distribution. Otherwise, when bending moment becomes prevalent, these differences between the cases of uniform and opposite moment distributions increase significantly but LCC^{15512} and $LCC^{EC3\text{-}1\text{-}3}$ are in these cases lower than LCC^{FEM}, as expected. Only the *general method* provides values lower than the elastic critical buckling load, being $\frac{LCC^{G.M.}}{LCC^{FEM}}$ ratio always lower than unity, but it could result very conservative if applied to routine upright rack design. It is worth to underline that the cross-section geometry in relation with the perforation systems of the T_upright is quite different from the ones of the most commonly used uprights and this is probably the reason for the failure of both cold-formed design approaches.

6. Concluding remarks

Thin-walled cold-formed members are used as uprights in steel storage pallet racks, which are vertical members forming the skeleton frame. The design of these key components, usually loaded by axial force and gradient moment, is quite complex because of the interactions between the different forms of instability. Their weight reflects directly on the cost of the whole rack system and, as a consequence, on its

Table 6
$\frac{LCC^{15512}}{LCC^{FEM}}$, $\frac{LCC^{EC3\text{-}1\text{-}3}}{LCC^{FEM}}$ and $\frac{LCC^{G.M.}}{LCC^{FEM}}$ ratios for the T_uprights.

e [mm]	ψ	$L = 2$ m			$L = 4$ m			$L = 5$ m		
		$\frac{LCC^{15512}}{LCC^{FEM}}$	$\frac{LCC^{EC3\text{-}1\text{-}3}}{LCC^{FEM}}$	$\frac{LCC^{G.M.}}{LCC^{FEM}}$	$\frac{LCC^{15512}}{LCC^{FEM}}$	$\frac{LCC^{EC3\text{-}1\text{-}3}}{LCC^{FEM}}$	$\frac{LCC^{G.M.}}{LCC^{FEM}}$	$\frac{LCC^{15512}}{LCC^{FEM}}$	$\frac{LCC^{EC3\text{-}1\text{-}3}}{LCC^{FEM}}$	$\frac{LCC^{G.M.}}{LCC^{FEM}}$
5		1.118	1.117	0.831	1.163	1.163	0.898	1.070	1.071	0.910
	0	1.118	1.117	0.831	1.163	1.163	0.898	1.070	1.070	0.910
	−1	1.118	1.117	0.831	1.163	1.163	0.898	1.070	1.070	0.910
10	1	1.047	0.972	0.818	1.103	1.027	0.891	1.049	0.978	0.906
	0	1.063	0.997	0.821	1.121	1.062	0.891	1.076	1.022	0.928
	−1	1.063	0.999	0.818	1.128	1.077	0.891	1.041	0.998	0.904
50	1	0.993	0.893	0.806	1.071	0.966	0.887	1.042	0.942	0.903
	0	1.023	0.931	0.815	1.089	1.005	0.885	1.094	1.013	0.949
	−1	1.014	0.926	0.805	1.096	1.022	0.884	1.015	0.951	0.898
100	1	0.835	0.704	0.751	1.007	0.850	0.867	1.019	0.860	0.888
	0	0.923	0.782	0.843	0.983	0.841	0.852	1.216	1.044	0.950
	−1	0.768	0.652	0.713	0.922	0.799	0.841	0.877	0.763	0.862
150	1	0.799	0.674	0.723	0.992	0.836	0.857	1.011	0.852	0.880
	0	0.923	0.776	0.878	0.941	0.793	0.830	1.317	1.109	0.930
	−1	0.637	0.535	0.631	0.827	0.699	0.804	0.810	0.686	0.832
500	1	0.789	0.672	0.710	0.986	0.840	0.852	1.009	0.858	0.876
	0	0.934	0.791	0.894	0.921	0.776	0.816	1.385	1.165	0.853
	−1	0.579	0.489	0.581	0.788	0.663	0.780	0.788	0.663	0.814
5000	1	0.789	0.711	0.687	0.982	0.882	0.841	1.009	0.905	0.867
	0	0.986	0.877	0.915	0.892	0.783	0.784	1.565	1.368	0.827
	−1	0.508	0.450	0.489	0.761	0.659	0.725	0.802	0.691	0.775

competitiveness on the market, stressing out the importance of an optimal design in terms of use of material resources and structural safety.

Three different European design procedures have been discussed in the present paper: the pallet rack code [19], the part 1-3 of EC3 for cold-formed members [22] and the *general method* described in part 1-1 of EC3 [6]. As shown, a substantial difference between these three different alternatives is due to the way of accounting for the buckling interaction between axial load and bending moments: only the *general method* considers correctly the influence of the axial load on the buckling moment while the formers assume a non conservative elastic buckling domain, as shown in Fig. 8. Waiting for a more accurate definition of this critical domain, a conservative proposal should be the approximation of the domain via a straight line passing through the critical axial load of the column, $N_{cr}(M = 0)$, and the lateral buckling moment of the beam, $M_{cr}(N = 0)$, which are both required for the beam–column verification checks.

Isolated members have been considered by selecting a wide range of cases, differing for geometry and perforations of the cross-section, member slenderness and load conditions. If reference is made to the codes properly recommended for cold formed rack members, the domain associated with the EN 15512 approach results the more favorable than the one obtained via EC3 part 1-3. Both these approaches need however urgent revision in order to consider appropriately the critical buckling interaction occurring in beam–columns. Furthermore, it is worth to mention that in case of T_uprights, which have cross-section geometry and perforation system significantly different from that of the other uprights, both the cold formed approaches are unconservative, being the load carrying capacity of columns and of beam–column with limited axial load eccentricity greater than the elastic buckling load. Additional cases have been considered for the T_upright under compression, by varying the effective length (L) from 1 m to 5 m and considering different steel grades [47]: S275, S350 and

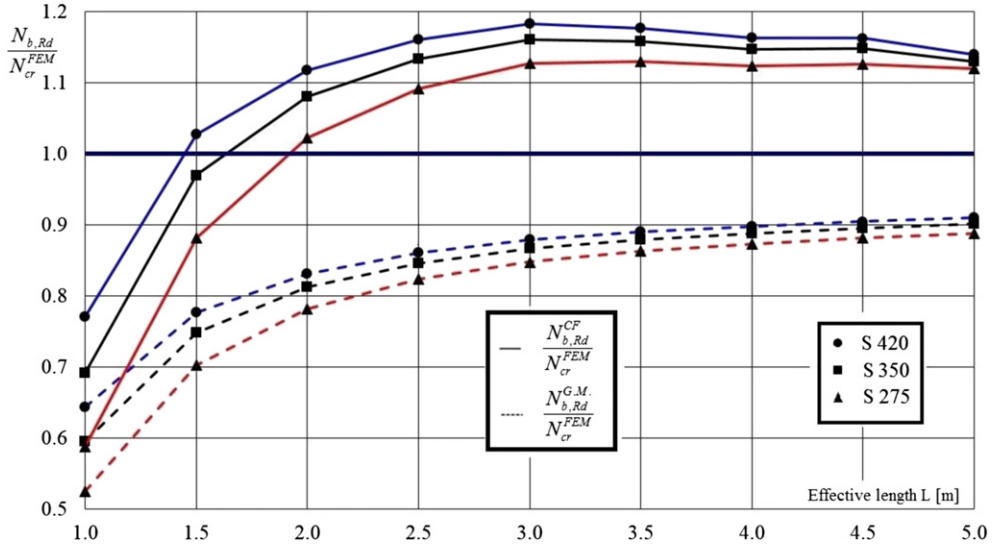

Fig. 22. $\frac{N_{b,Rd}^{CF}}{N_{cr}^{FEM}}$ and $\frac{N_{b,Rd}^{G.M.}}{N_{cr}^{FEM}}$ ratios versus the effective length of T_upright columns.

S420, which are the grades most commonly used for uprights. The main results are plotted in Fig. 22, where the values of the design axial resistance associated with the general method ($N_{b,Rd}^{G.M.}$) and with the ones of cold formed approaches ($N_{b,Rd}^{CF} = N_{b,Rd}^{15512} = N_{b,Rd}^{EC3\text{-}1\text{-}3}$) are presented over the critical buckling (N_{cr}^{FEM}), plotting the ratios $\frac{N_{b,Rd}^{G.M.}}{N_{cr}^{FEM}}$ and $\frac{N_{b,Rd}^{CF}}{N_{cr}^{FEM}}$ versus the effective length L for the T_upright column. A similar trend can be noted for all the plotted curves: by increasing the buckling length and the steel grade, the plotted ratios increase too. Furthermore, as to the traditional cold-formed design approaches, it can be noted that the $\frac{N_{b,Rd}^{CF}}{N_{cr}^{FEM}}$ values are not greater than unity only for the lowest values of L. If reference is made to values of the effective length of interest for routine design and typical of racks with inter-story level and/or upright frame panel of great height, the overestimation of the load carrying capacity with respect to the elastic buckling load becomes non-negligible (up to 20%, approximately), confirming the need of urgent investigations to define more accurately the scope of both EN 15512 and EC3-1-3 approaches. Otherwise, the *general method*, which leads to an increment of the member performances only in a limited number of cases, appears to be the one which can be used safely to design uprights.

Finally, it should be noted that no attention is herein directly paid to the seismic design, despite the fact that the proposed research outcomes should however be directly used also to guarantee adequate safety levels under earthquakes, dealing with the stability verification checks independently from the nature of the applied loads.

References

[1] Godley MHR. Design of cold formed steel members. In: Rhodes, editor. Elsevier Applied Science; 1991. p. 361–99.
[2] Dinis PB, Young B, Camotin D. Local–distortional interaction in cold-formed steel rack-section column. Thin-Walled Struct 2014;81:185–95.
[3] Vlasov VZ. Thin walled elastic beams. 2nd ed. Jerusalem: Israel Program for Scientific Transactions; 1961.
[4] Timoshenko SP, Gere JM. Theory of elastic stability. 2nd ed. New-York: McGraw Hill; 1961.
[5] Chen WF, Atsuta T. Theory of beam–columns: vol. 2 space behaviour and design. McGraw Hill; 1977.
[6] CEN. Eurocode 3 — design of steel structures — part 1-1: general rules and rules for buildings. CEN European Committee for Standardization; 2005.
[7] Bernuzzi C, Rugarli P. A unified approach for the design of columns and beam–columns cold-formed members. Part 1: the approach, n. 5. Costruzioni Metalliche; 2009 [in English].
[8] Bernuzzi C, Rugarli P. A unified approach for the design of columns and beam–columns cold-formed members. Part 2: validation of the approach, n. 6. Costruzioni Metalliche; 2009 [in English].
[9] Szabo IF, Dubina D. Recent research advances on the ECBL approach. Part II: interac-tive buckling of perforated sections. Thin-Walled Struct 2004;42:195–210.
[10] Shanmugam NE, Thevendran V, Tan YH. Design formula for axially compressed perforated plates. Thin-Walled Struct 1999;34:1–20.
[11] El-Sawy KM, Nazmy AS, Martini MI. Elasto-plastic buckling of perforated plates under uniaxial compression. Thin-Walled Struct 2004;42:1083–101.
[12] Moen CD, Schafer BW. Elastic buckling of thin plates with holes in compression or bending. Thin-Walled Struct 2009;47:1597–607.
[13] Dhanalakshmi M, Shanmugam NE. Design for openings in equal-angle cold-formed steel stub columns. Thin-Walled Struct 2001;39:167–87.
[14] Shanmugam NE, Dhanalakshmi M. Design for openings cold-formed steel channels stub columns. Thin-Walled Struct 2001;39:961–81.
[15] Eccher G, Rasmussen KJR, Zandonini R. Geometric nonlinear isoparametric spline finite strip analysis of perforated thin-walled structures. Thin-Walled Struct 2009;47:219–32.
[16] Casafont M, Pastor M, Bonada J, Roure F, Pekoz T. Linear buckling analysis of perforated steel storage rack columns with the finite strip method. Thin-Walled Struct 2012;61:71–85.
[17] Moen CD, Schafer BW. Direct strength design for cold-formed steel members with perforations. Research report. Baltimore, USA: Department of Civil Engineering, The Johns Hopkins University; march 2009 [http://www.moen.cee.vt.edu/postedfiles/AISI%20DSMHoles%20Report%20Final%20R2.pdf].
[18] Baldassino N, Zandonini R. Design by testing of industrial racks. Adv Steel Constr 2011;7(1):27–47.
[19] CEN, EN 15512. Steel static storage systems — adjustable pallet racking systems —principles for structural design. CEN European Committee for Standardization; 2009 137.
[20] RMI, MH 161. Specification for the design, testing and utilization of industrial steel storage racks. RMI — Rack Manufacturers Institute; 2008 59.
[21] Australian Standards, AS 4084. Steel storage racking. Australia: AS Standards; 2012.
[22] European Committee for Standardization, CEN. Eurocode 3 — design of steel structures — part 1-3: design of cold formed members. Brussels: CEN; May 2005.
[23] Bernuzzi C, Pieri A, Squadrito V. Warping influence on the monotonic design of unbraced steel storage pallet racks. Thin-Walled Struct 2014;79:71–82.
[24] Bernuzzi C, Gobetti A, Gabbianelli G, Simoncelli M. Warping influence on the resistance of uprights in steel storage pallet racks. J Constr Steel Res 2014;101:224–41.
[25] Bernuzzi C, Simoncelli M. European design approaches for isolated cold-formed thin-walled beam–columns with mono-symmetric cross-section. Eng Struct 2015; 86:225–41.
[26] CEN, ENV 1993-1-1. Eurocode 3 — design of steel structures, part 1-1: general rules and rules for building. CEN European Committee for Standardization; 1992.
[27] Boisssonnade N, Greiner G, Jaspart JP, Lindner J. Rules for member stability in En 1993-1-1: background documentation and design guidelines. ECCS document n. 119 — technical committee 8 — stability; 2006.
[28] Machado SP. Interaction of combined loads on the lateral stability of thin-walled composite beams. Eng Struct 2010;32:3516–27.
[29] Mohri F, Bouzerira C, Potier-Ferry M. Lateral buckling of thin-walled beam–column elements under combined axial and bending loads. Thin-Walled Struct 2008;46: 290–302.
[30] Bijlard F, Feldmann M, Naumes J, Sedlacek G. In: Ernst, Sohn, editors. The "general method" for assessing the out-of-plane stability of structural members and frames in comparison with alternative rule in En 1993 — Eurocode 3 — part 1-1, 3. Steel Construction; 2010 [No. 1].
[31] Szalai J., "The "general method" of EN 1993-1-1", NSC April 2011, pp. 30–31.
[32] Papp F. Global stability analysis using general method. www.consteelsoftware.com/files/sharedUploads/Pdf/General_stability_analysis.pdf.
[33] Castiglioni CA, Kanyilmaz A, Angeretti M, Brambilla G, Chiarelli GP, Bernuzzi C. Experimental results of full scale push over tests of project SEISRACK2 (seismic behaviour of steel storage pallet racking systems). 2nd European Conference on Earthquake Engineering, Istanbul Aug. 25–29, 2014; 2014.
[34] Erkem RE. Shear deformable hybrid finite-element formulation for buckling analysis of thin-walled members. Finite Elem Anal Des 2014;82:33–45.
[35] Nedelcu M. Buckling mode identification of perforated thin-walled members by using GTB and shell FEA. Thin-Walled Struct 2014;82:67–81.
[36] Adany S. Flexural buckling of simply-supported thin-walled columns with consider-ation of membrane shear deformations: analytical solutions based on shell model. Thin-Walled Struct 2014;74:36–48.
[37] Nascimbene R. Towards non-standards numerical modeling of thin-shell structures: geometrically linear formulation. Int J Comput Methods Eng Sci Mech 2014;15: 126–41.
[38] Hsiao KM, Lin WY. A co-rotational formulation for thin-walled beams with monosymmetric open section. Comput Methods Appl Mech Eng 2000;190:1163–85.
[39] Teh LH. Cubic beam elements in practical analysis and design of steel frames. Eng Struct 2001;23:1243–55.
[40] Battini JM, Pacoste C. Co-rotational beam elements with warping effects in instability problems. Comput Methods Appl Mech Eng 2002;191:1755–89.
[41] Turkalj G, Brnic J, Prpic-Orsic J. Large rotation analysis of elastic thin-walled beam-type structures using ESA approach. Comput Struct 2003;81:1851–64.
[42] Chen HH, Lin WY, Hsiao KM. Co-rotational finite element formulation for thin-walled beams with generic open section. Comput Methods Appl Mech Eng 2006; 195:2334–70.
[43] El Fatmi R. Non-uniform warping including the effects of torsion and shear forces. Part I: a general beam theory. Int J Solids Struct 2007;44:5912–29.
[44] Saritas A. Modeling of inelastic behavior of curved members with a mixed formula-tion beam element. Finite Elem Anal Des 2009;45:357–68.
[45] Sapountzakis EJ, Dourakopoulos JA. Flexural–torsional postbuckling analysis of beams of arbitrary cross section. Acta Mech 2010;209(1–2):67–84.
[46] ABAQUS®/STRAND. User's manual version 6.8. USA: Hibbitt, Karlsson and Sorensen; 2006.
[47] CEN EN 10025. Hot rolled products of structural steels — parts 1–6. CEN European Committee for Standardization; 2009 137.